Astron. Astrophys. 362, 1093–1108 (2000)

ASTRONOMY AND ASTROPHYSICS

VLBI observations of 6.7 and 12.2 GHz methanol masers toward high mass star-forming regions

I. Observational results: protostellar disks or outflows?

V. Minier, R.S. Booth, and J.E. Conway

Onsala Space Observatory, 439 92 Onsala, Sweden

Received 16 May 2000 / Accepted 31 August 2000

Abstract. We present VLBI observations of 6.7 and 12.2 GHz methanol masers in 14 star-forming regions, namely NGC 7538, S 252, W 75N, W 48, G 31.28+0.06, S 231, S 255, S 269, Mon R2, G 9.62+0.20, Cep A, W 51, G 59.78+0.06 and G 29.95-0.02. In 10 of these sources, the methanol masers show elongated morphologies in the VLBI map and exhibit linear velocity gradients. These linear structures have lengths of 50 to 1300 AU. We consider whether these structures are consistent with circumstellar disks. Assuming that we see the whole diameter of a Keplerian disk then we derive sub-solar central masses with the exception of W 48. However, it is possible that we only see masers in a fraction of the disk which lies in front of a young massive star. Assuming that the Keplerian disks have diameters of 1000 AU, then the derived enclosed masses vary from 1 to 75 $M_{\odot}$. We suggest that other models such as accelerating outflows could explain the linear structures; proper motions are needed in order to discriminate between the possible models.

Key words: masers – techniques: interferometric – stars: circumstellar matter – stars: formation – ISM: H II regions

1. Introduction

6.7 and 12.2 GHz methanol masers are generally seen toward star-forming regions. Recent surveys have confirmed that 6.7 and 12.2 GHz methanol masers are usually detected in regions exhibiting typical signposts of massive star formation, e.g H_2O and OH maser sites (Caswell et al. 1993, 1995) and IRAS sources satisfying the Wood & Churchwell criteria (Wood & Churchwell 1989) for ultra compact HII (UCHII) regions (Walsh et al. 1997; Slysh et al. 1999). These masers are usually extremely bright and have flux densities from a few tens to a few thousands of Jy. For instance, the 6.7 GHz masers are more than 10 times stronger on average than their galactic OH maser counterparts (Caswell et al. 1995). For these reasons, i.e close association with star formation and strong emission, 6.7 and 12.2 GHz methanol masers appear to be appropriate tools for probing star-forming regions using interferometric techniques.

Send offprint requests to: V. Minier (vincent@oso.chalmers.se)

Previous high resolution imaging of 6.7 and 12.2 GHz methanol maser sources has been conducted in the Southern hemisphere using the Australia Telescope Compact Array (ATCA) at 6.7 GHz and the Parkes-Tidbinbilla Interferometer (PTI) at 12.2 GHz. Norris et al. (1988, 1993, 1998) and Phillips et al. (1998) found that in many sources, the 6.7 and 12.2 GHz maser features were aligned and exhibited linear velocity gradients. They argued that the linear structures were consistent with rotating disks of masers seen edge-on. The derived values of the radii of these disks and the approximate enclosed masses deduced by assuming Keplerian rotation, were 500 to 2000 AU and 3 to 100 $M_{\odot}$, respectively. These results agreed with theoretical models of accretion disks around massive stars (Lin & Pringle 1990), but the values of the enclosed mass depended heavily on the estimation of the radius of the disks. Furthermore, when both 6.7 and 12.2 GHz masers were present in a given source, similar velocity features were found to be spatially coincident. Walsh et al. (1998) also observed that 36 out of 97 6.7 GHz methanol maser sites were linearly extended and in some cases exhibited linear velocity gradients along many of these lines of maser features. The derived values of enclosed mass were in some cases too high making the model of Keplerian rotation of masers around massive stars inconsistent. Walsh et al. (1998) suggested that 6.7 GHz methanol masers instead arose behind shock fronts.

We began a Northern hemisphere campaign to observe methanol masers in 1997 when several telescopes of the European VLBI Network (EVN) were equipped with 6.7 GHz receivers. Minier et al. (1998, 1999) used the EVN and the VLBA, respectively to observe NGC 7538, W 75N and S 252 at 6.7 and 12.2 GHz. A few years earlier, Moscadelli et al. (1999) had observed the 12.2 GHz methanol masers in W 3(OH) using the VLBA. In all cases, alignments of maser components were found which exhibit linear velocity gradients, although in some sources e.g W 3(OH) additional components were distributed more randomly. In order to clarify the nature of the 6.7 and 12.2 GHz methanol maser sites, i.e to investigate the possibility that these masers arise from ordered structures such as disks or shocks, we have conducted further VLBI observations at 6.7 and 12.2 GHz toward 14 star-forming regions. We have

Table 1. Summary of the methanol maser observations. The coordinates are either from our VLBI observations presented in this paper (ref. 1), or are the observed positions taken from Menten (1991; ref. 2), Caswell et al. (1995; ref. 3) and Phillips (priv. comm., ref. 4). The flux density peak is from Menten (1991) and Caswell et al. (1995)

Source	Epoch		Coordinates (J2000)		Flux density peak (Jy)		Ref.
name	6.7 GHz	12.2 GHz	RA(h m s)	Dec(^{o} $'$ $''$)	6.7 GHz	12.2 GHz	
NGC 7538	Nov. 98	Nov. 98	23:13:45.364	61:28:10.55	346	198	1
S 252	May 97	Jul. 97	06:08:53.7	21:38:30	495	235	2
W 48	May 97	Jul. 97	19:01:45.5	01:13:28	560	109	3
G 31.28+0.06	May 97	Jul. 97	18:48:12.7	-01:26:36	80	140	3
W 75N	May 97	–	20:38:36.8	42:37:59	1080	0	2
S 231	Nov. 98	–	05:39:13.059	35:45:51.29	208	0	1
S 255	Nov. 98	–	06:12:54.024	17:59:23.01	72	0	4
S 269	Nov. 98	–	06:14:36.7	13:49:41	61	1.3	2
Mon R2	Nov. 98	–	06:07:47.9	-06:22:57	337	4.2	3
G 9.62+0.20	–	Nov. 98	18:06:14.8	-20:31:32	5090	180	3
Cep A	–	Jan. 99	22:56:18.095	62:01:49.45	1420	300	1
W 51	–	Nov. 98	19:23:39.429	14:31:04.65	33	21	1
G 59.78+0.06	–	Jan. 99	19:43:11.248	23:44:03.34	42	16	1
G 29.95-0.02	–	Jan. 99	18:46:03.741	-02:39:21.43	206	53	1

selected 14 strong methanol masers at 6.7 and 12.2 GHz observable with Northern hemisphere interferometers with good UV coverages. In this paper, we present these VLBI observations toward the following 14 well known star-forming regions: NGC 7538, S 252, W 75N, W 48, G 31.28+0.06, S 231, S 255, S 269, Mon R2, G 9.62+0.20, Cep A, W 51, G 59.78+0.06 and G 29.95-0.02. In Sect. 2, we describe our observations as well as the data reduction procedure. Maps of all the observed sources, derived physical parameters and comments on individual sources are given in Sect. 3. Discussion on the nature of the methanol maser sites, i.e if the CH_3OH masers are located in disks, behind shocks or in other regions, takes place in Sect. 4.

2. Observation and data analysis

The $5_1 \rightarrow 6_0 A^+$ transition at 6668.518 MHz and the $2_0 \rightarrow 3_{-1}$E transition at 12178.595 MHz are the two strongest methanol masers. In the Northern hemisphere only the EVN is equipped to observe the 6.7 GHz transition while only the VLBA can observe at 12.2 GHz, so both arrays were used. The 6.7 GHz EVN observations were conducted in May 1997 and November 1998 (3 antennas in 1997: Onsala, Effelsberg and Medicina; 5 antennas in 1998: Onsala, Effelsberg, Medicina, Torun and Jodrell Bank). The star-forming regions observed at 6.7 GHz were NGC 7538, W 75N, W 48, G 31.28+0.06, S 252, S 231, S 269, S 255, and Mon R2. The VLBA observations at 12.2 GHz were conducted in July 1997, November 1998, and January 1999 (all antennas in 1997 and 1998; 9 antennas in 1999). The star-forming regions observed at 12.2 GHz were NGC 7538, S 252, W 48, 31.28+0.06, G 29.95-0.02, G 9.62+0.20, G 59.78+0.06, CepA, and W 51. Many of these sources exhibited both 6.7 and 12.2 GHz masers, but they were not systematically observed at both frequencies. In Table 1, we summarise our observations, i.e the name of the observed sources (Column 1), the epochs of observations (Columns 2,3), the coordinates of the sources in J2000 (Columns 4, 5), and the flux densities expected from single dish observations (Columns 6,7).

Slighty different observing strategies were used during the VLBI campaigns. In 1997 a typical observing sequence with both the EVN and VLBA was 13 minutes on a strong calibrator for the purpose of band-pass, delay and rate calibration, followed by 39 minutes on the maser source. Observations on a given source were repeated 5 to 7 times depending on the source declination. During the EVN and VLBA observations in 1998 and 1999, we modified our observing strategy in order to better determine the absolute position of the methanol maser sites. Observing blocks of 44 minutes were repeated over 24 hours for the EVN experiment in 1998, and over 12 hours for the VLBA experiments in 1998 and 1999. Each 44 minute observation started with the observation of a strong continuum calibrator, followed by the observations of a methanol maser alternating with a compact and close continuum source for the purpose of phase referencing. For the EVN observations, about 10 scans of 11 minutes and about 15 scans of 5 minutes were taken on each methanol maser source and on the nearby compact continuum source, respectively. For the VLBA observations, about 16 scans of 6 minutes and about 25 scans of 3 minutes were taken on each methanol maser source and on the nearby compact continuum source, respectively.

The methanol maser spectra generally span 10 km s^{-1}, usually contain features separated by $\sim$1 km s^{-1} and having minimum FWHM of $\sim$0.2 km s^{-1} (e.g Caswell et al. 1995). Therefore we used a bandwidth of 0.5 MHz at 6.7 GHz (covering 22 km s^{-1}), and a bandwidth of 1 MHz at 12.2 GHz (covering 25 km s^{-1}). Observations at both 6.7 and 12.2 GHz were recorded in VLBA modes and correlated on the NRAO correlator using 512 channels in 1997 and 1024 channels in 1998 at 6.7 GHz, and 256 channels in 1997 and 512 channels in 1998 and 1999 at 12.2 GHz. The corresponding velocity resolutions were 0.04 and 0.02 km s^{-1} at 6.7 GHz, and, 0.1 and 0.05 km s^{-1} at 12.2 GHz, respectively.

The data were calibrated and reduced using the Astronomical Image Processing System (AIPS) and the DIFMAP package.

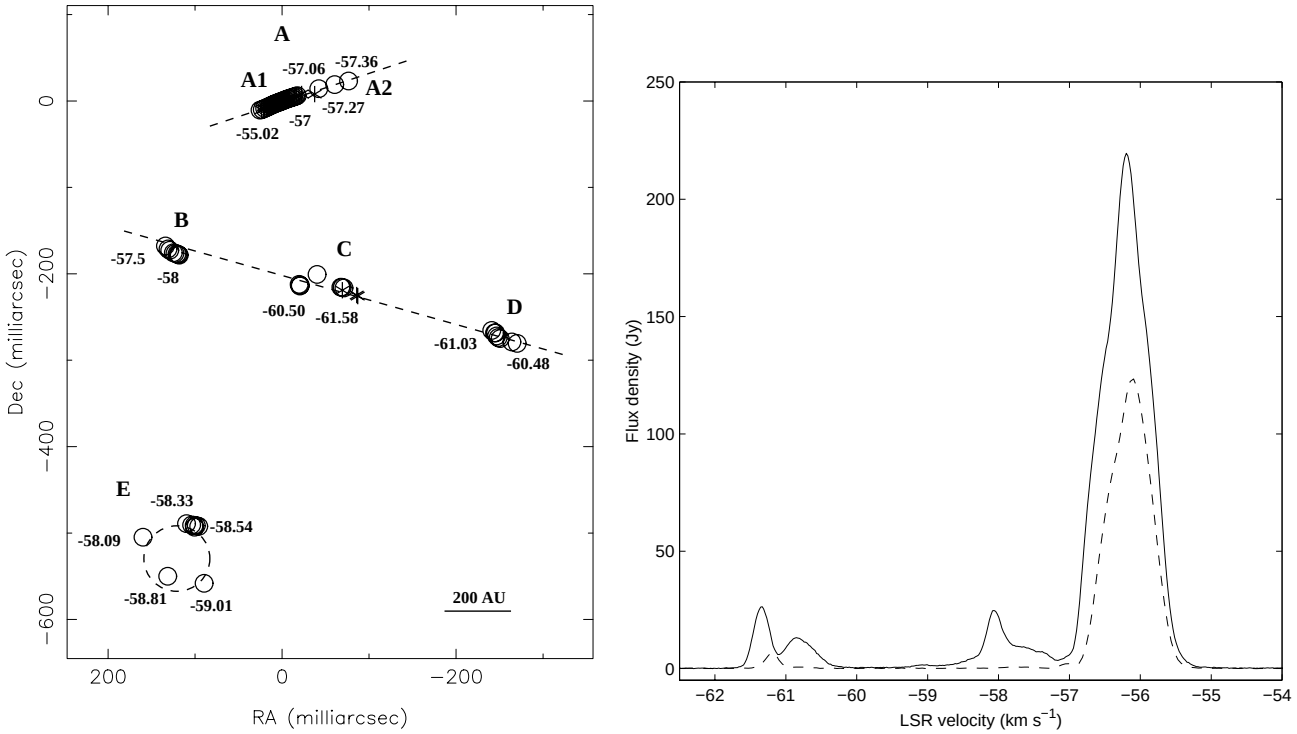

Fig. 1. NGC 7538: Map of 6.7 GHz (circles) and 12.2 GHz (stars) methanol masers and spectra at 6.7 GHz (full line) and 12.2 GHz (dashed line). Values in the map give LSR velocities of maser features. Dashed lines and/or circles in the VLBI map show interesting geometrical structures.

Standard calibration, fringe-fitting and imaging procedures to analyse spectral line VLBI data were used (Reid 1995). Similar reduction techniques were applied to all sources at both of the frequencies. The bandpass corrections were determined by using strong continuum calibrators in the AIPS task BPASS. Doppler corrections were ensured by running the tasks SETJY and CVEL. The amplitude calibration was derived from the total power spectra of methanol masers using ACFIT. The determination of the residual delay, and the first calibration of the fringe-rate were estimated by using strong continuum calibrators as source models in FRING. Complementary phase calibration, using CALIB, were applied to the phase referenced 1998 and 1999 data using the observations of the compact continuum source before and after the spectral line sources. The data were then self-calibrated in order to remove the residual fringe-rates that were not corrected by the first run of FRING. For this purpose, we used a strong maser component within a single channel, that was believed to arise from a single, compact and spatially isolated maser. This was used as a single point source model in FRING. The derived corrections were applied to all the other channels. Further self-calibrations were achieved by self-calibrating the data in DIFMAP with cleaned images of the reference channel. Each group of channels corresponding to different features in the methanol maser spectra were mapped using DIFMAP and the AIPS task FRMAP in order to estimate their positions by making large images of $\sim$2-5 arcsec^2. Finally, using the AIPS tasks IMAGR and JMFIT, we imaged, with higher spatial resolution (image size, 512$\times$512, pixel size, 2 and 0.2 mas at 6.7 and 12.2 GHz, respectively), the emissions in every channel and found their relative positions from the position of the reference channel by applying elliptical Gaussian fits around the peak emission. We found that the relative positions of the masers agreed within a few mas with their "pre-located" positions determined in the FRMAP and DIFMAP maps. We can set up a lower and upper limit to the error in relative position of 5μas and 1 mas depending on the size of the maser "spots" and the signal-to-noise ratio derived from Gaussian fit. For 2 sources in 1997 at 6.7 GHz, W 48 and G 31.28+0.06 the declination error in relative position may be much larger than 1 mas because of poor UV coverage due to low declination. We were able to find absolute positions for 6 sources by applying standard imaging techniques (IMAGR and JMFIT) to the data fringed and phase referenced with an external calibrator source. We expect that the dominant contribution to errors in absolute position is that of the unmodelled atmosphere, and depends on the angular separations of the calibrators and maser sources. At 6.7 GHz, the positions of a few EVN antennas may also be a major source of errors. We estimate an upper limit of 30 mas error based on the continuum calibrator fringe-rates.

3. Results and comments on individual sources

In this section, we present VLBI maps of each of the 14 methanol maser sources that we observed using the EVN and VLBA. For each source (Figs. 1 to 14), we give the cross-power spectra (scalar averaging) taken on the shortest VLBA baseline Los Alamos-Pie Town at 12.2 GHz and on the EVN baseline Effelsberg-Onsala at 6.7 GHz, as well as the VLBI maps of the

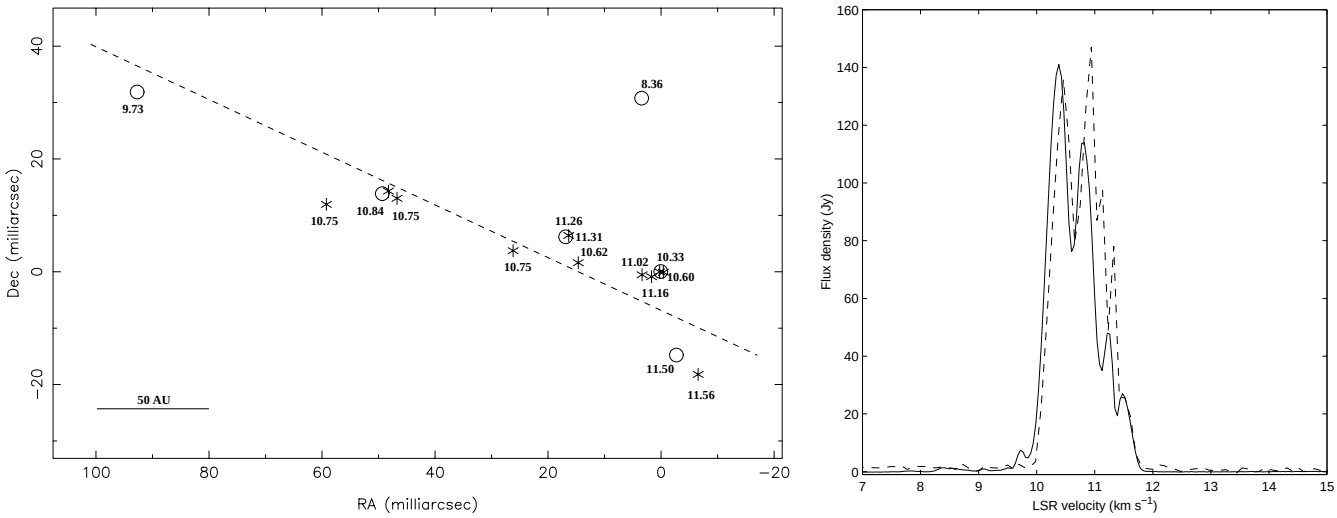

Fig. 2. S 252: Map of 6.7 GHz (circles) and 12.2 GHz (stars) methanol masers and spectra at 6.7 GHz (full line) and 12.2 GHz (dashed line)

masers. For each VLBI map, the plotted position of a maser component is the averaged position of velocity channel emissions within 2 mas^2 and 1 mas^2 at 6.7 GHz and 12.2 GHz, respectively. It corresponds in most of the cases to average velocity channels over $\sim$0.2 km s^{-1}, i.e the typical FWHM of methanol maser features. The averaging method shows clearly the overall structure of each maser source. In addition, it identifies sub-groups of maser components well separated (more than a few mas) from each other. However, this way of averaging the positions breaks the extended masing regions into separate spots in the case of sources having a continuous distribution of maser components. The nature of the maser distribution within a specific cluster of masers will be clarified in the comments on individual sources in order to differentiate between large structures of separate maser components and continuous distributions of maser components corresponding to broad spectral features. All the given positions are relative to the reference channel positions located at the origin of the map. The available absolute position of this reference feature is given in Table 1.

3.1. NGC 7538

The 6.7 and 12.2 GHz methanol masers in NGC 7538-IRS 1 were observed in May and July 1997, and imaged by Minier et al. (1998). We give here the results of the new observations from November 1998. 6.7 and 12.2 GHz masers are grouped in 5 clumps labelled A,B,C,D and E. 12.2 GHz masers are spatially coincident with 6.7 GHz masers when both occur in A and C. Masers in A lie along a line of $\sim$280 AU in extent. This line of masers is more extented at 6.7 GHz than at 12.2 GHz. We suggest that the 6.7 and 12.2 GHz masers in A1 arise from a single radius of an edge-on disk as interpreted by Minier et al. (1998) while 6.7 GHz masers in A2 lie in the same disk but at different radii. That is indicated by different velocity gradients. A1 masers exhibit a clear linear velocity gradient suggesting rotating masers at a constant radius, while A2 masers fall onto a slighty different line. Note that the maser components are continuously distributed within A1. Indeed 6.7 GHz masers trace a more extended region in radius than 12.2 GHz masers in A. It is expected from theoretical models that 6.7 GHz masers can occur in a wider range of density or larger range of radii in a disk than 12.2 GHz masers (Sobolev et al. 1997). B, C, and D also define a line of three maser clumps that do not exhibit any velocity gradient. Finally new masers have been detected in E which were not observed in the earlier observations of Minier et al. (1998). They roughly form a circle that may coincide with the circular structure seen in the 15 GHz continuum map (see Minier et al. 1998).

3.2. S 252

S 252 is an extended HII region excited by an O6.5 V star and located at a distance of 2.2 kpc (Haikala 1995). It contains massive star-forming regions such as S 252A, B and C. The methanol maser source is probably associated with the far-infrared source GL5180 (Snell et al. 1988). The 6.7 and 12.2 GHz methanol masers delineate a line of masers, with a roughly linear velocity gradient along it (Fig. 2) despite a few masers following a different velocity distribution. The whole linear structure is extended over 120 mas or 270 AU. A weak isolated maser feature lies north of the line.

3.3. W 48

W 48 is a galactic HII region lying at a distance of 3.4 kpc (Vallée et al. 1990). Toward this source Wood & Churchwell (1989) detected a strong UC HII region, G 35.2-1.74, that is believed to be a site of massive star formation and which has associated OH, and CH_3OH masers (Caswell et al. 1995). Unfortunately, the absolute position of the CH_3OH masers is not known within an accuracy better than a few arcsec. Nevertheless, they are probably located at the position of a strong inonised region, W 48A, imaged by Onello et al. (1994). The methanol maser spectra at 6.7 and 12.2 GHz present a double peaked profile

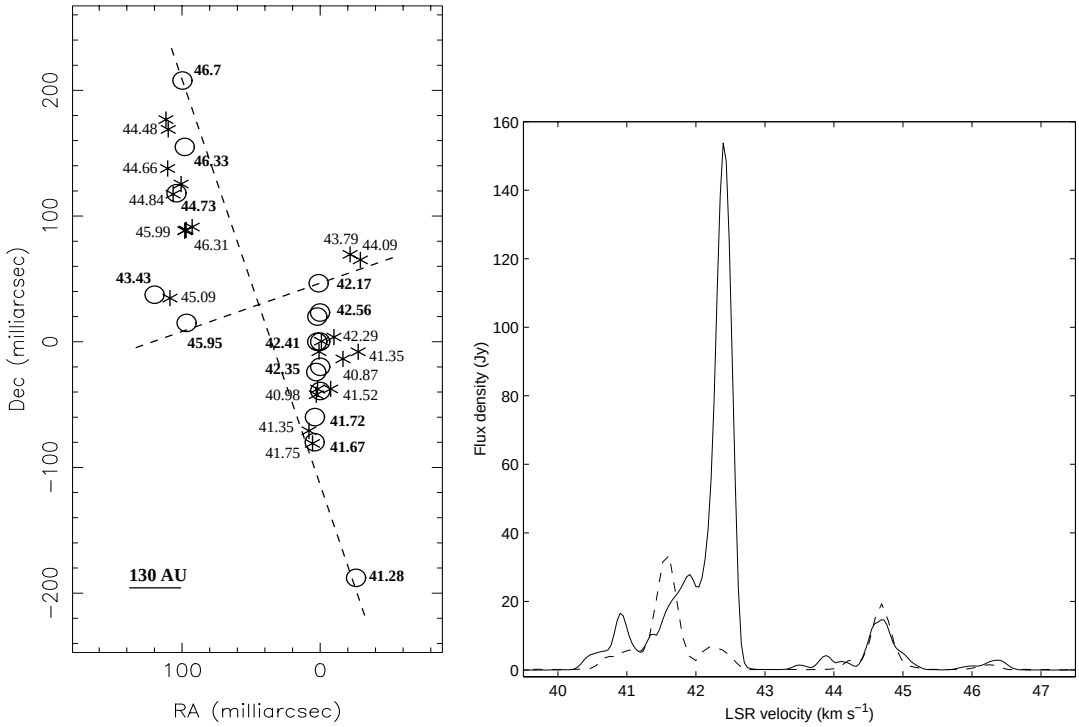

Fig. 3. W 48: Map of 6.7 GHz (circles) and 12.2 GHz (stars) methanol masers and spectra at 6.7 GHz (full line) and 12.2 GHz (dashed line)

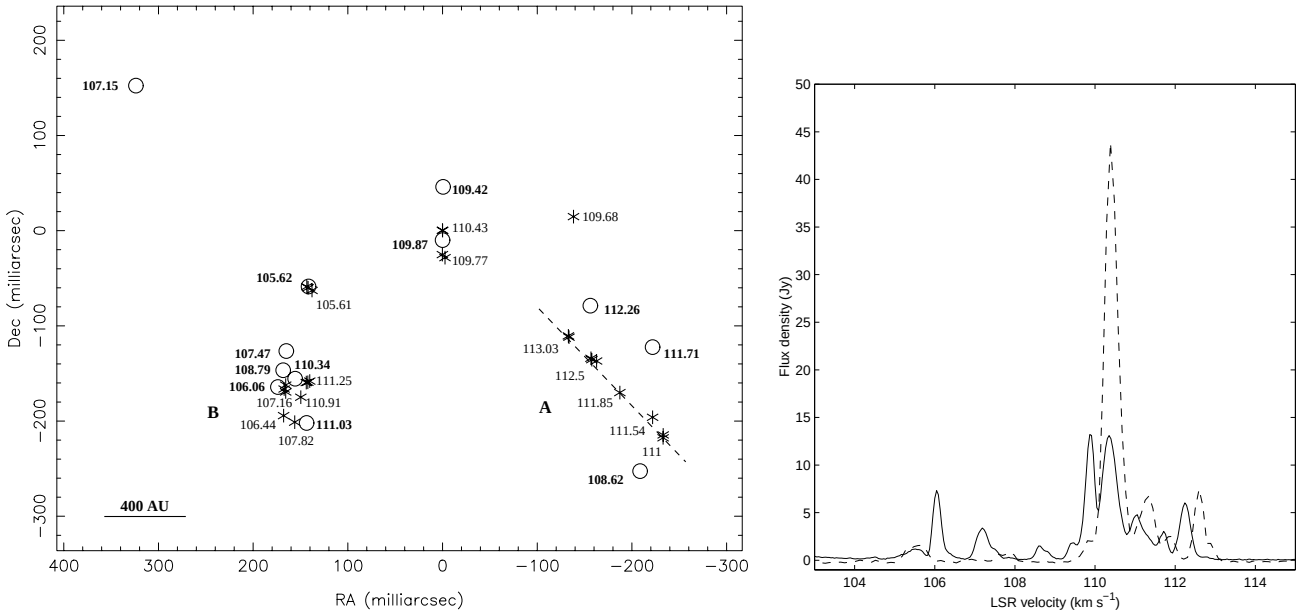

Fig. 4. G 31.28+0.06: Map of 6.7 GHz (circles) and 12.2 GHz (stars) methanol masers and spectra at 6.7 GHz (full line) and 12.2 GHz (dashed line)

(Fig. 3). The masers producing the lower velocity features (from 40.15 to 42.56 km s^{-1}) are located south from the East-West dashed line in Fig. 3. The higher velocity masers (from 43.43 to 46.70) lie north from the same axis. The masers are distributed along a direction North-South illustrated by the long dashed axis in Fig. 3.

3.4. G 31.28+0.06

G 31.28+0.06 is an UC HII region located at 5.6 kpc in the giant HII region W 43 (Kurtz et al. 1994; Blum et al. 1999). It is also closely associated with other typical signposts of massive star formation such as CH_3OH and OH masers (Caswell et al. 1995; Walsh et al. 1998). The spectra of the 6.7 and 12.2 GHz methanol masers show many features over 10 km s^{-1} (Fig. 4),

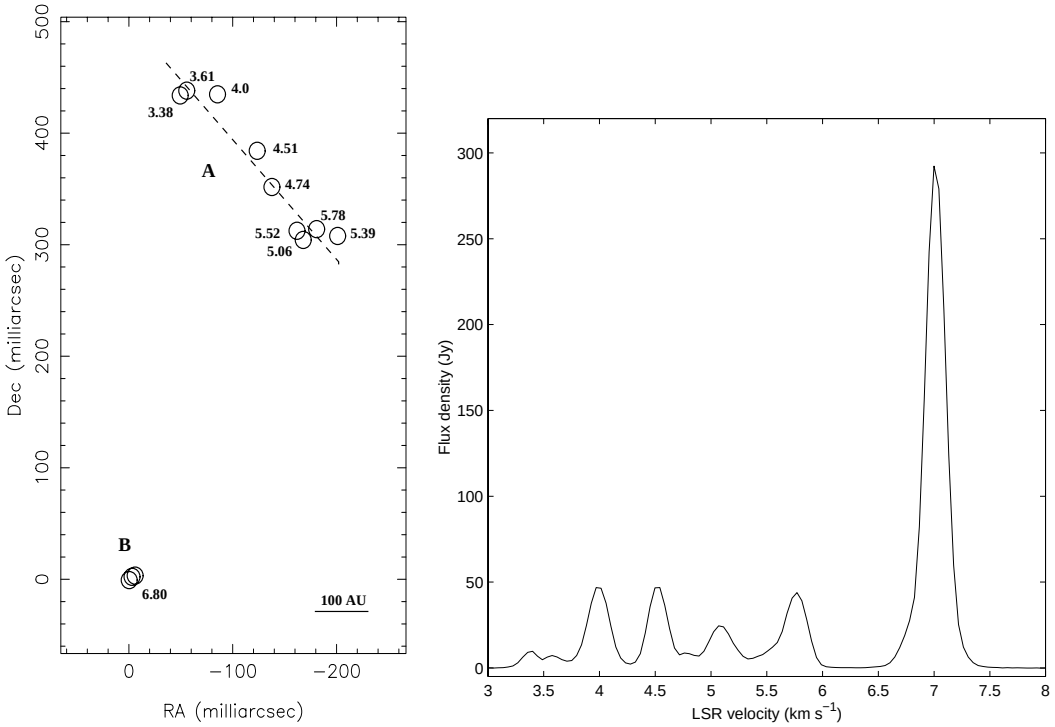

Fig. 5. W 75N: Map of 6.7 GHz methanol masers (circles) and spectrum at 6.7 GHz (full line)

the 12.2 GHz emission being stronger than the 6.7 GHz masers. The corresponding VLBI map is complex. The masers are organised in 2 clusters (A and B in Fig. 4), 3 isolated and single components, and one pair of features at the center of the map. Note that despite their large uncertainities in declination offset, the 6.7 GHz masers draw approximately the same pattern as the 12.2 GHz masers. The aligned group of masers A is 150 mas or 780 AU in extent, and has a linear velocity gradient.

3.5. W 75N

W 75N is a very active region of massive star formation exhibiting OH, H_2O masers (Haschick et al. 1981; Hunter et al. 1994; Torelles et al. 1997). The 6.7 GHz methanol masers fall into two groups in the VLBI map (Fig. 5). Group A corresponds to the 8 features between 3 and 6 km s^{-1} in the spectrum in Fig. 5. Group B corresponds to the strongest emission. A and B are separated by $\sim$400 mas or 800 AU at a distance of 2 kpc. Group A is located at the North-East of the position of VLA1 in Torelles et al. (1997). Furthermore, the elongated structure of group A seems to be aligned with the linear structure of OH and H_2O masers found by Torelles et al. (1997) and Baart et al. (1986) that is believed to trace outflows from VLA1 (W 75N(Ba)). Group A also exhibits a linear velocity gradient along a line of 380 AU in extent.

3.6. S 231

The 6.7 GHz methanol maser site S 231 lies in the region of star formation S 235 at a distance of 2.5 kpc (Caswell et al. 1995; Israel & Felli 1978). The spectrum contains many features over the velocity range -11 to -15 km s^{-1} (Fig. 6). The masers are grouped into three clusters A, B and C in the VLBI map (Fig. 6). A is an elongated structure of 40 mas or 100 AU, with a clear velocity gradient along it.

3.7. S 255

The 6.7 GHz methanol masers arise from the high-mass star-forming region S 255 IR embedded within the optical HII region complex S 254-S 257 (Caswell et al. 1995; Miralles et al. 1997). Three compact HII regions were detected toward S 255 IR (S 255-2a, S 255-2b and S 255-2c by Snell & Bally, 1986) and one UC HII region G 192.58-0.04 (Kurtz et al. 1994). The methanol masers are not associated with any detected compact HII region. The cross-power spectrum contains four features, three features centred around 4.8 km s^{-1} and one at 1.82 km s^{-1} corresponding to the groups of masers A and B, respectively in the VLBI map (Fig. 7). A and B are separated by $\sim$200 mas or 500 AU at a distance of 2.5 kpc.

3.8. S 269

The 6.7 GHz methanol masers in the HII region S 269 are probably associated with the young IRAS source 06117+1350 or S 269-IRS 2 that is powered by a massive young O star (Eiroa et al. 1994). This infrared source also shows OH and H_2O masers (Genzel & Downes 1977), but does not have any UC HII region emission (Kurtz et al. 1994). The methanol masers fall into two distinct groups separated by 60 mas or 240 AU at a distance of

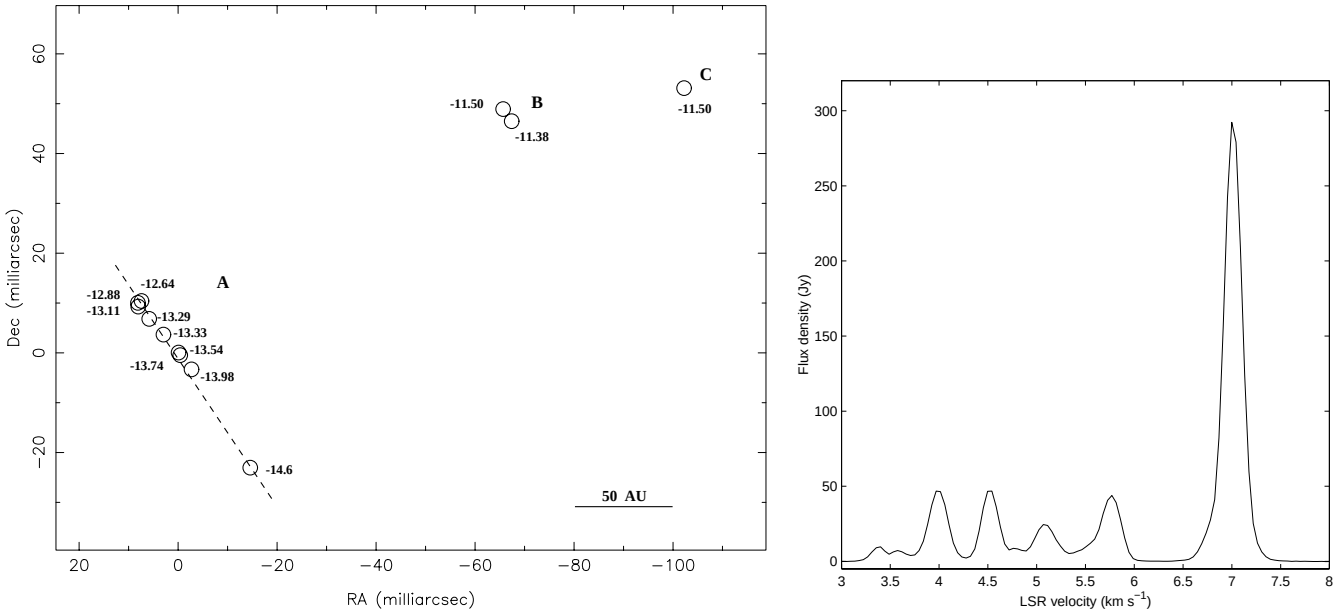

Fig. 6. S 231: Map of 6.7 GHz methanol masers (circles) and spectrum at 6.7 GHz (full line)

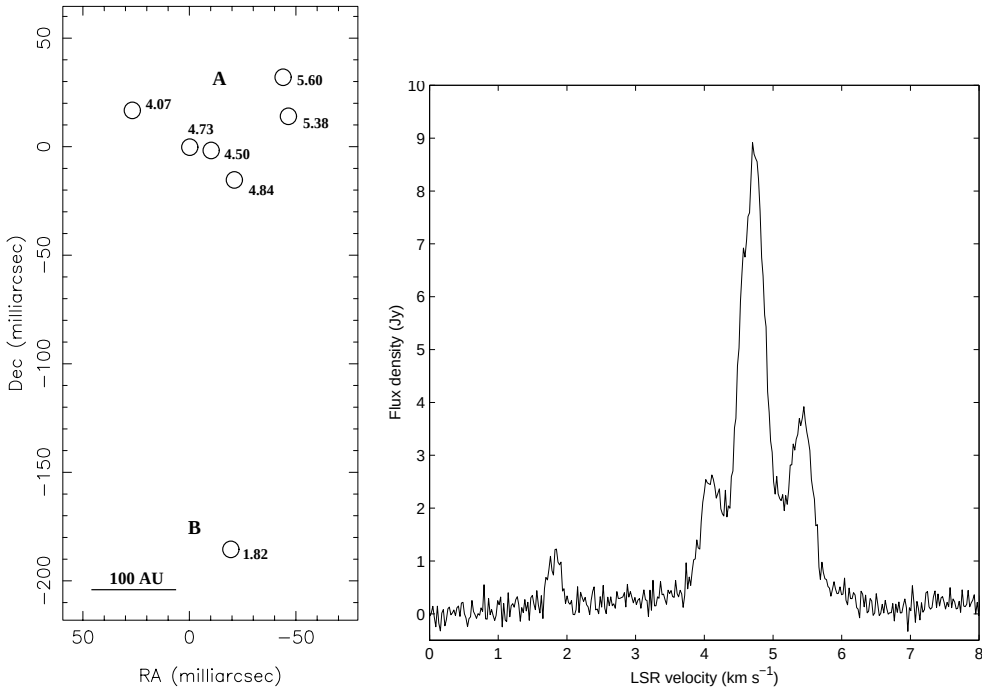

Fig. 7. S 255: Map of 6.7 GHz methanol masers (circles) and spectrum at 6.7 GHz (full line)

4 kpc (Fig. 8). Group A corresponds to the weak feature centred at 14.7 km s^{-1} (Fig. 8) and is very compact while group B delineates a linear structure of ∼14 mas or 55 AU in extent, and show a clear linear velocity gradient.

3.9. Mon R2

The Monoceros R2 stellar cluster is a huge massive star-forming region located at a distance of only 830 pc; it has been extensively studied by Carpenter et al. (1997). Our observations at 6.7 GHz show that the spectrum of the methanol masers contain at least five features over 3 km s^{-1} (Fig. 9). The masers fall onto a linear structure 170 mas or 130 AU in extent in the VLBI map.

3.10. G 9.62+0.20

G 9.62+0.20 is an HII region complex located at 5.7 kpc. One of the UC HII regions, component E in Hofner et al. (1996), is associated with the strongest 6.7 GHz methanol maser that was imaged by Phillips et al. (1998). The 12.2 GHz methanol maser

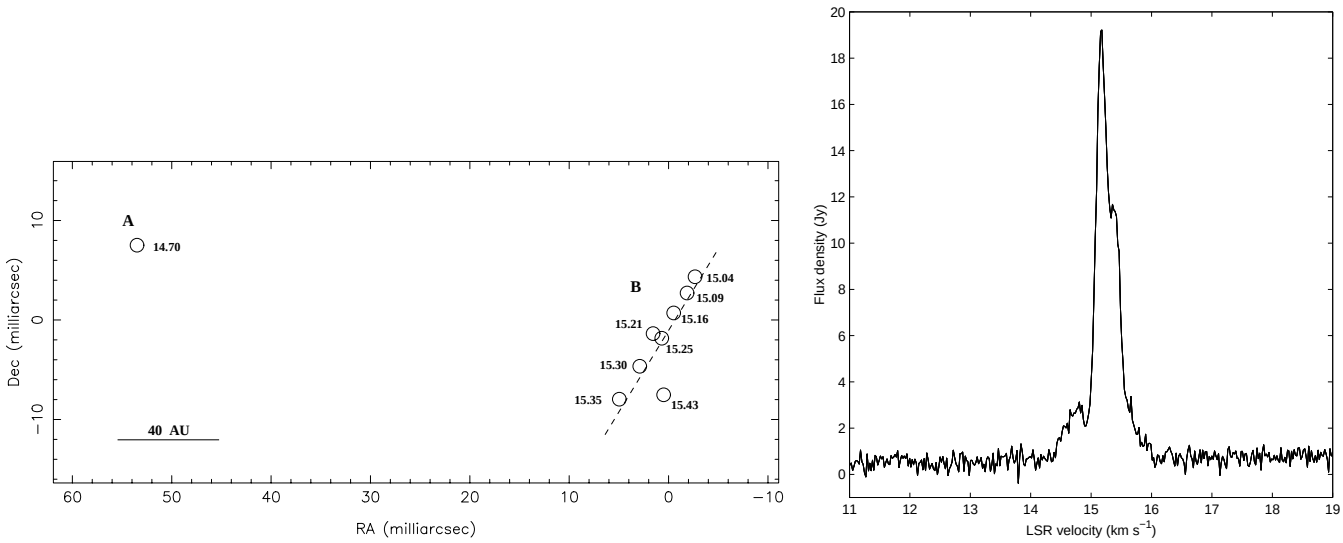

Fig. 8. S 269: Map of 6.7 GHz methanol masers (circles) and spectrum at 6.7 GHz (full line)

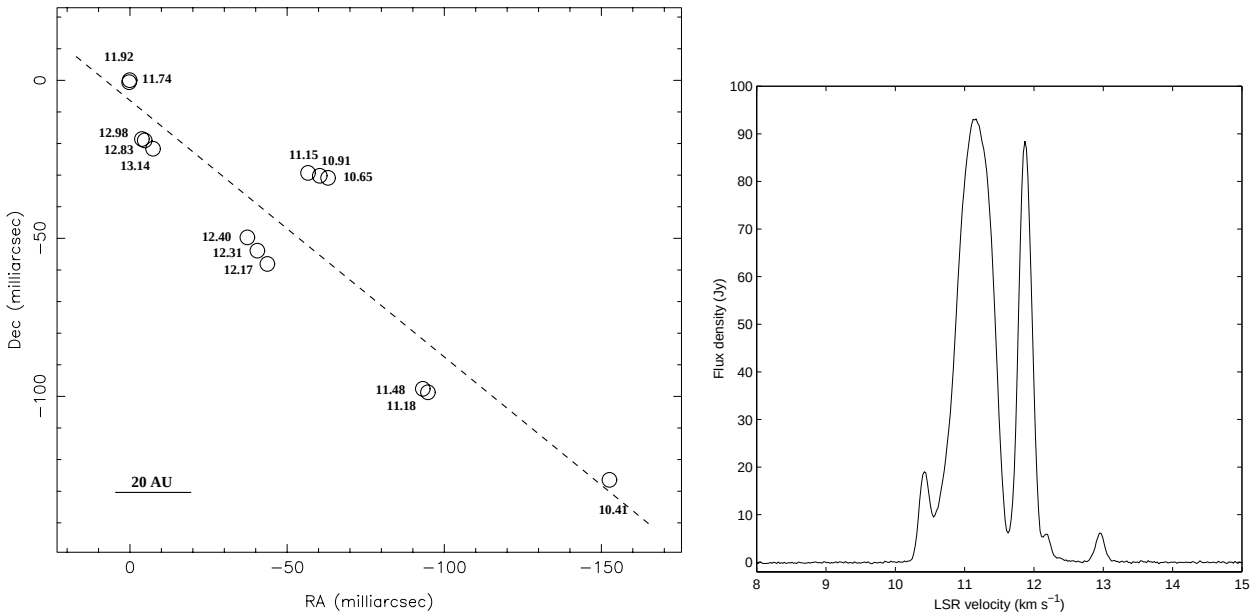

Fig. 9. Mon R2: Map of 6.7 GHz methanol masers (circles) and spectrum at 6.7 GHz (full line)

is much weaker, but its spectrum is still very rich in features (Fig. 10). The 12.2 GHz maser components fall onto two lines of masers. Note that the maser components are continuously distributed within A, B, C, E, F, G and H. The clusters A, B, and C form indeed a linked masing region with a linear velocity gradient along it, while the other clusters are well isolated and separated structures. The angular distance between the lines is $\sim$100 mas corresponding to 570 AU at a distance of 5.7 kpc. This is typically the diameter of the UC HII region of component E that is ionised by a type B1 ZAMS (Hofner et al. 1996; Testi et al. 1998).

3.11. Cep A

The CO condensation, Cepheus A (CepA), contains many massive star-forming regions. One of them, the UC HII region CepA-HW 2 (Hughes 1985) is associated with H_2O, OH and CH_3OH masers. The H_2O masers delineate an ordered structure that is thought to be a rotating disk of 800 mas or 600 AU in extent at a distance of 730 pc (Torelles et al. 1996). The OH masers are spherically distributed around the UC HII region and spread over a larger region of 2 arcsec (Migenes et al. 1992). The 12.2 GHz CH_3OH masers are organised into three clumps in the VLBI maps corresponding to three features in the spectra (Fig. 11). The velocities of the CH_3OH masers are approximately the same as the velocities of the OH masers located

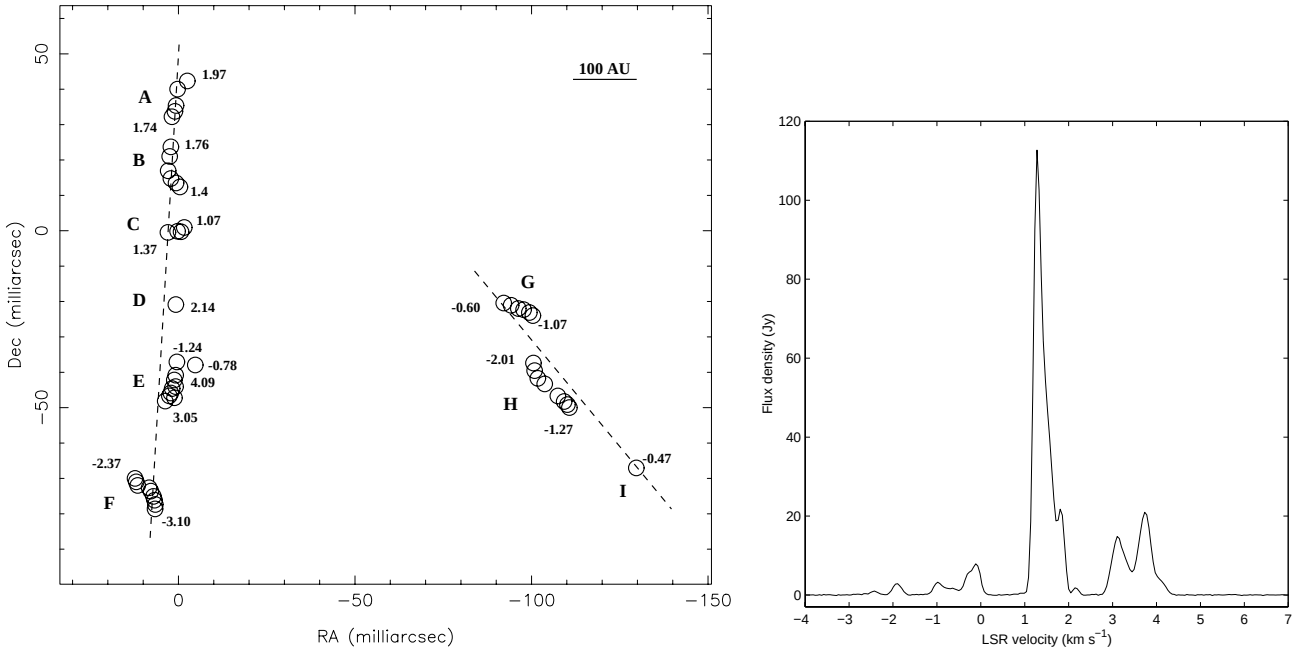

Fig. 10. G 9.62+0.20: Map of 12.2 GHz methanol masers (circles) and spectrum at 12.2 GHz (full line)

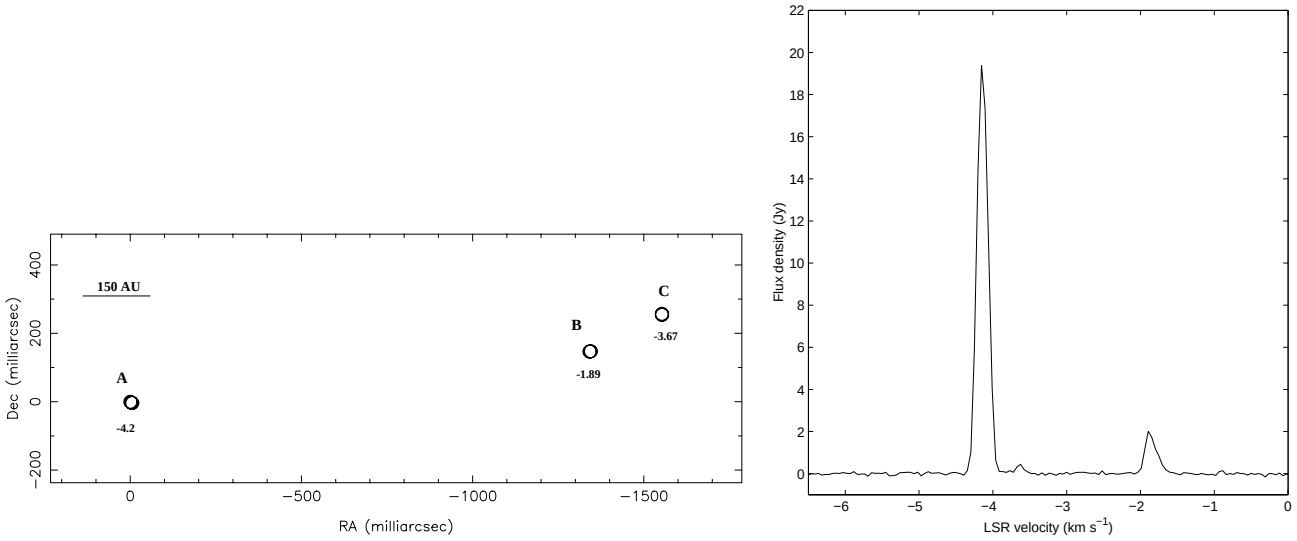

Fig. 11. Cep A: Map of 12.2 GHz methanol masers (circles) and spectrum at 12.2 GHz (full line)

at similar positions. Therefore, the 12.2 GHz methanol masers are probably associated with the OH maser shell.

3.12. W 51

W 51 is one of the most luminous sites of massive star formation in our galaxy. It is located at a distance of 7.5 kpc. It contains a large number of O and B stars in formation. W 51 is divided into three regions, W 51A, W 51B and W 51C (Carpenter & Sanders 1998). The methanol maser sites G 49.49-0.37 and G 49.49-0.39 (Caswell et al. 1995) in W 51A are associated with W 51-North and W 51e1/e2, respectively. We observed G 49.49-0.37 which is located within the massive giant molecular cloud G 49.5-0.2 (83×114 pc) and is coincident with OH, H_2O and NH_3 masers (Zhang et al. 1998). The spectrum of this 12.2 GHz methanol maser contains a single feature spanning from 55.6 to 56.24 km s^{-1}, that may be resolved in 2 distinct features (Fig. 12). It corresponds in the VLBI channel map to a linear structure of $\sim$9.5 mas or 70 AU in extent, with a clear velocity gradient along it (Fig. 12). The maser components are indeed continuously distributed along the linear structure.

3.13. G 59.78+0.06

This methanol maser source (Caswell et al. 1995) is associated with the young star-forming region CO 59.79+0.84 which

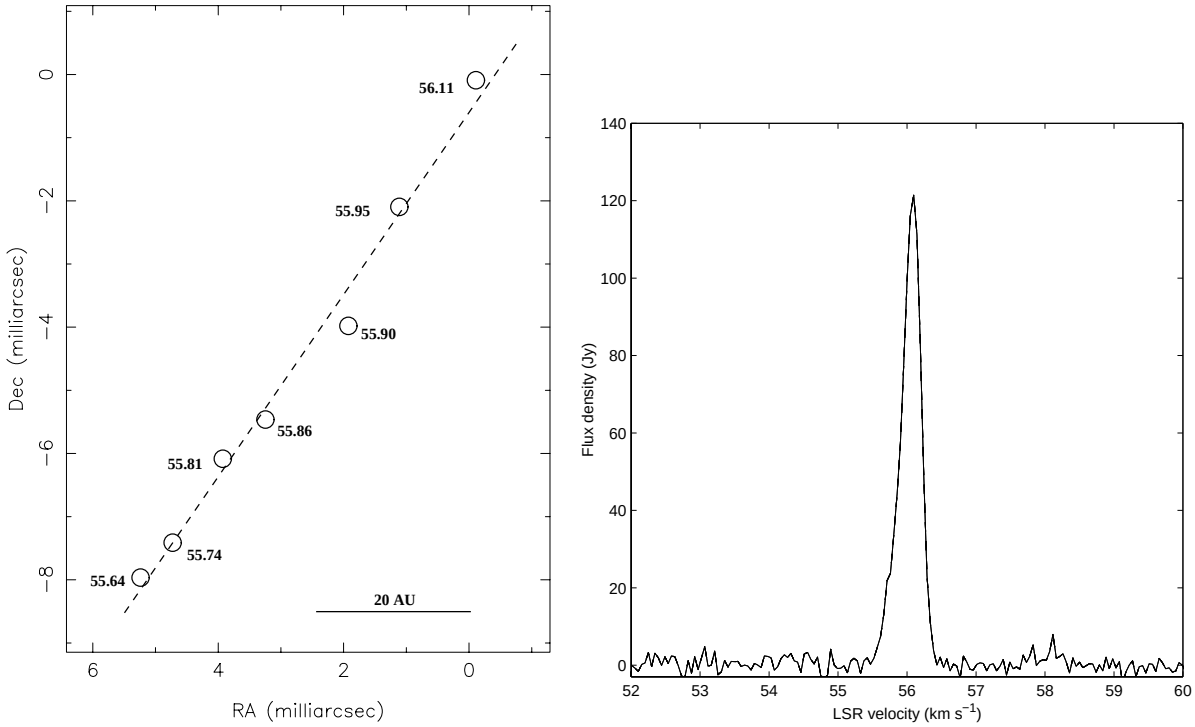

Fig. 12. W 51: Map of 12.2 GHz methanol masers (circles) and spectrum at 12.2 GHz (full line)

also contains H_2O and OH masers (Lada et al. 1981; Braz & Sivagnaman 1987). The spectrum consists of two features centred at 16.98 and 26.89 km s^{-1}, that form two clusters of a few mas in extent separated by 700 mas (Fig. 13). The position of the 12.2 GHz CH_3OH masers coincides with the OH and H_2O masers. No UC HII regions were detected toward G 59.78+0.06 by Kurtz et al. (1994) despite its association with an IRAS source (19410+2336) satisfying the color criteria for UC HII region (Wood & Churchwell 1989). Kurtz et al. (1994) have suggested that such sources are heated either by low mass stars or by young massive protostars. In the first case, no ionised region would be produced, while in the second case the radio continuum from an UC HII region would be too weak to be detectable. Note that the spectrum of the 6.7 GHz methanol maser in G 59.78+0.06 contains many other features between 16.98 and 26.89 km s^{-1}.

3.14. G 29.95-0.02

G 29.96-0.02 is an UC HII region located at a distance of 9 kpc (Wood & Churchwell 1989), and is powered by a O7 star (Watson & Hanson 1997). The methanol maser site G 29.95-0.02 (Caswell et al. 1995; Menten 1991) coincides with the H_2O masers and a NH_3 hot core, but is slighty offset by a few arcsec from the continuum peak of the UC HII region (Cesaroni et al. 1998). The NH_3 hot core is believed to be a signpost of an embedded high mass star in early stage of its formation, before the UC HII region phase since no radio continuum emission has been detected. In addition, a velocity gradient along the NH_3 core structure suggests that a rotating disk like structure is present at the location of the methanol and water masers (Cesaroni et al. 1998). The cross-power spectrum of the 12.2 GHz masers contains a broad feature spanning 95.4 to 95.6 km s^{-1}, that is a blend of at least two components (Fig. 14). The masers describe a clear linear structure of 10 mas or 85 AU in extent, with a linear velocity gradient along it. The maser components are continuously distributed along the linear structure although they are represented as well separate spots in the Fig. 14.

4. Discussion

4.1. Summary of the results

In Sect. 3, we have presented observations of 6.7 and 12.2 GHz methanol masers toward 14 sources. All these sources are associated with regions of massive star formation, and most of the methanol masers are associated with a detected UCHII region. We classify our methanol maser structures into four categories as similarly defined by Phillips et al. (1998) and Norris et al. (1998); *linear* defines a source in which the masers form a line; a source is defined as *elongated* if the masers are mainly distributed along a single position angle; a source is *complex* if no large and ordered structure can be found; and finally a source is *simple* if it only contains a few isolated maser spots. Some sources have ambiguous classifications, e.g G 31.28+0.06. To avoid any confusion, we call a source *linear* when at least one linear morphology dominates the whole structure. In our sample of 14 sources, 2 sources are *simple* (Cep A and G 59.78+0.06), 2 sources are *complex* (G 31.28+0.06 and S 255), 1 source is *elongated* (W 48), and the 9 other sources are *linear*. Within the *linear* sources, 7 of them exhibit a linear velocity gradient along the line of components. Additionally, W 48 (*elongated*) and Mon R2

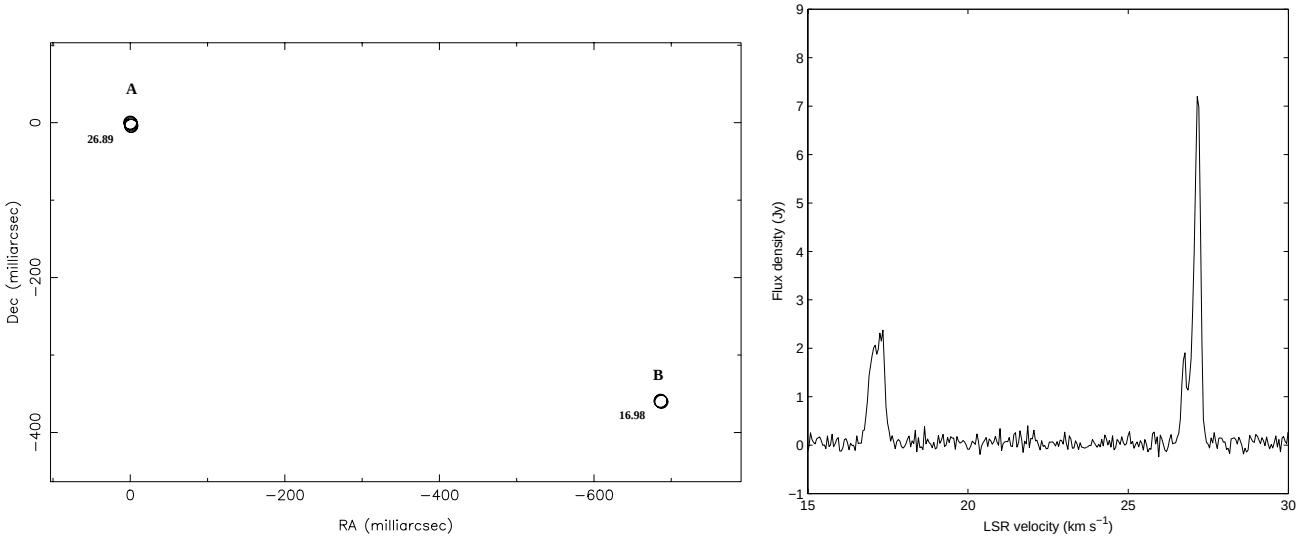

Fig. 13. G 59.78+0.06: Map of 12.2 GHz methanol masers (circles) and spectrum at 12.2 GHz (full line)

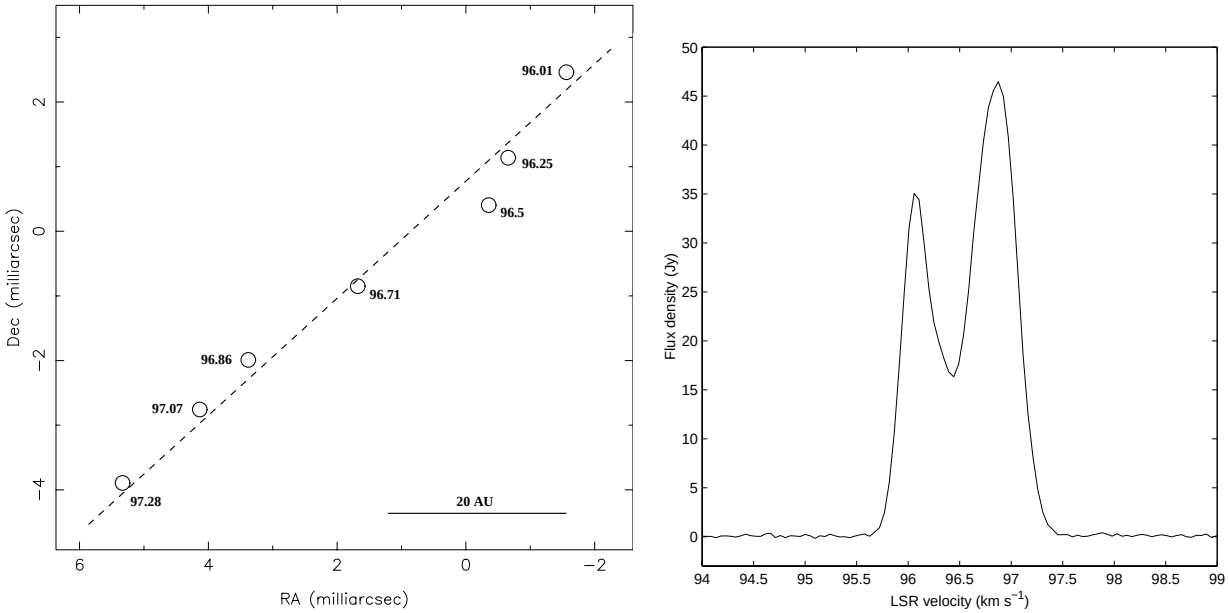

Fig. 14. G 29.95-0.02: Map of 12.2 GHz methanol masers (circles) and spectrum at 12.2 GHz (full line)

(*linear*) also show blue and redshifted masers, i.e masers approaching and receding. Finally, there is a line of masers with a linear velocity gradient within the *complex* morphology of G 31.28+0.06. In total in our sample of 14 sources, we detect linear velocity gradients in 10 regions. Position-velocity diagrams for these 10 cases are shown in Figs. 15 and 16. The properties of these linear structures are presented in Table 2. The measured velocity gradients span about a factor of 10; and excluding the largest and smallest gradients the remaining sources show only a factor of 3 variation in velocity gradient.

4.2. Do the methanol masers trace disks?

A number of possible models such as accelerating outflows and edge-on rotating disks can be constructed to explain the lines

Table 2. Measured parameters of the linear structures of masers. $\frac{dv}{dx}$ is obtained by linear fitting of v-x plot in Figs. 15 and 16. The length is the linear extent of each line of masers

Source	Length(AU)	$\frac{dv}{dx}$(km s^{-1} AU^{-1})
NGC 7538	280	9.1×10^{-3}
S 252	240	5.5×10^{-3}
W 48	1300	11.4×10^{-3}
G 31.28+0.06	780	2×10^{-3}
W 75N	380	5.6×10^{-3}
S 231	95	17.2×10^{-3}
S 269	55	6.5×10^{-3}
Mon R2	130	23×10^{-3}
W 51	70	5.7×10^{-3}
G 29.95-0.02	85	14.8×10^{-3}

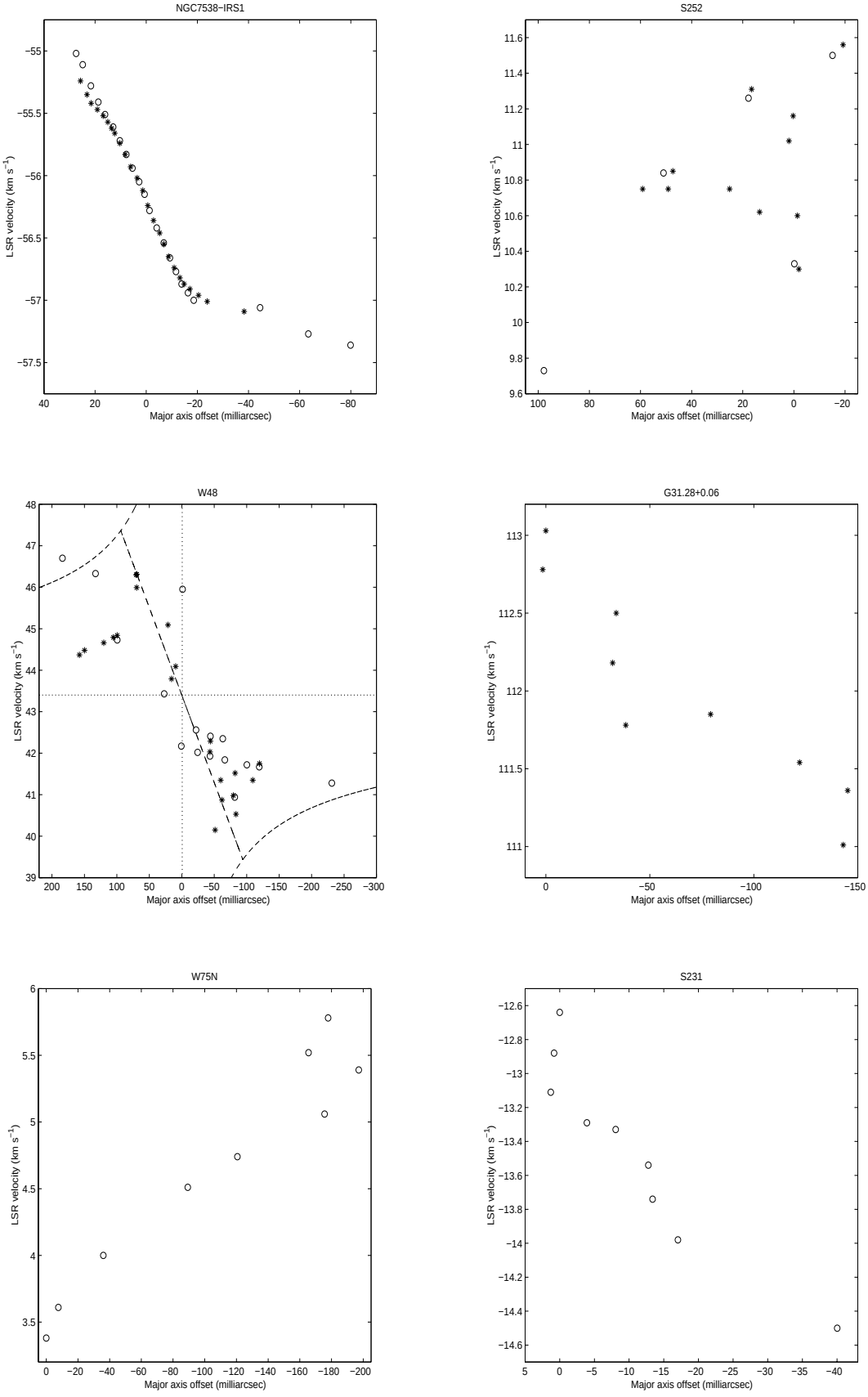

Fig. 15. v-x diagram of NGC 7538, S 252, W 48, G 31.28+0.06, W 75N, S 231, where the major axis position is the position of the maser projected onto the dashed line in the respective maps. 6.7 GHz and 12.2 GHz masers are represented by circles and stars, respectively.

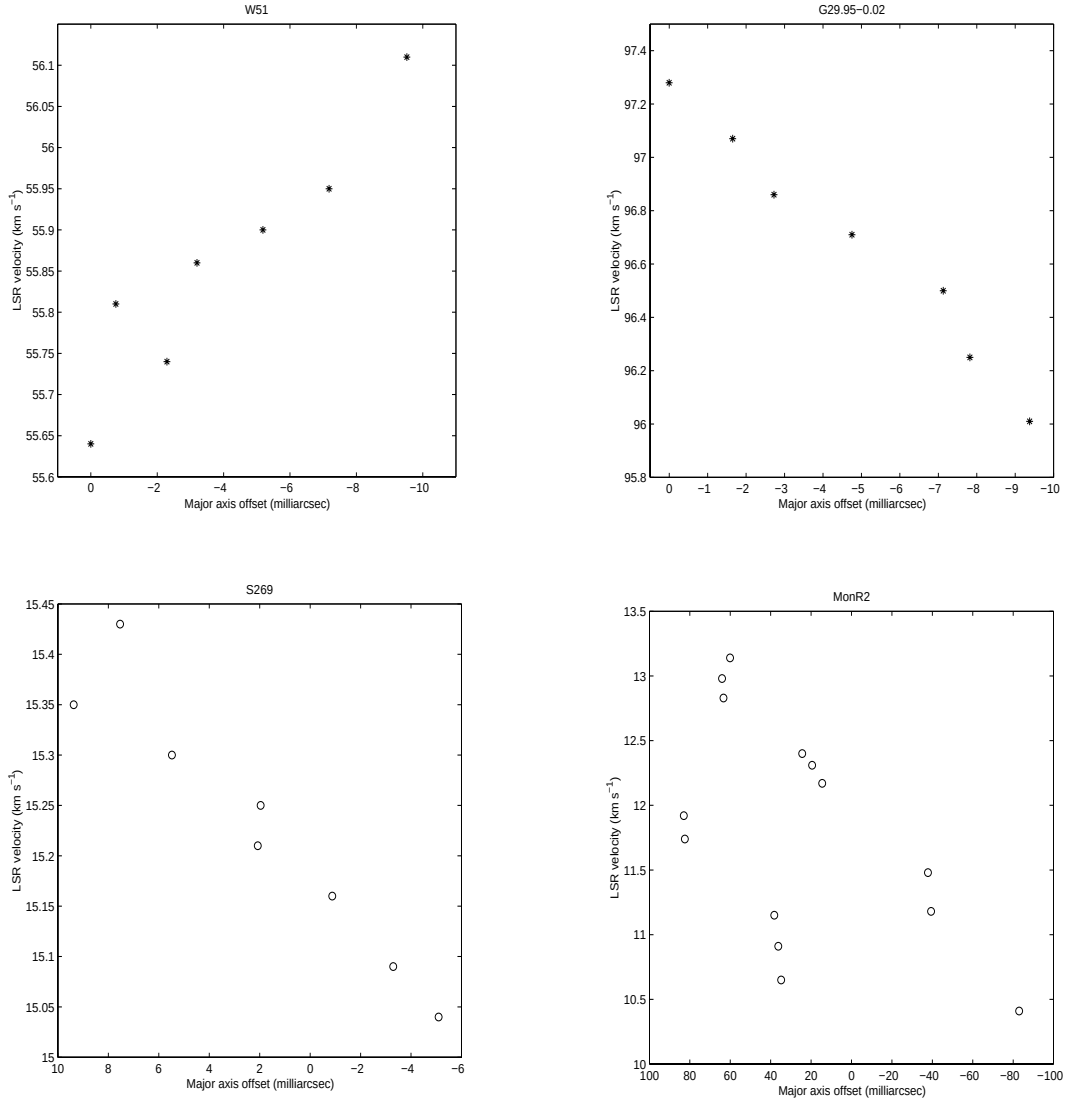

Fig. 16. v-x diagram: W 51, G 29.95-0.2, S 269, Mon R2. 6.7 GHz and 12.2 GHz masers are represented by circles and stars, respectively

of masers with linear velocity gradients. Nevertheless the relatively narrow ranges of size and velocity suggest a common mechanism. It has been argued by Norris et al. (1998) that edge-on Keplerian disks most naturally explain the observed linear velocity gradients. Here we investigate this explanation to see if the required disk sizes and central masses are reasonable. Other possible explanations (shocks, outflows) of the data are considered in Sect. 4.5

We argue that 10 methanol masers sources have morphologies and velocity distributions satisfying the rotating disk model illustrated in Fig. 17. For such a rotating disk seen nearly edge-on the line of sight velocity is,

$$v = V_{rot} \times \frac{x}{r} \times cosi + v_{sys} \quad (1)$$

where V_{rot} is the rotational velocity, r is the radius of the circle of masers, v_{sys} is the systemic velocity, i is the inclination angle of the disk and x is the linear distance in projection from the stellar position (see Fig. 17). If the disk is edge-on, i is zero. The line of sight velocity is, in the case of rotating disk of masers at constant radius around a newly formed star, a linear function of x (Fig. 17d). If the methanol masers lie within an annular region over a range of radii, then each ring of masers around the central star at a radius r is associated with a line in velocity vs major axis offset (v-x) diagram. Thus the clear linear velocity gradients in the v-x diagrams, as seen in NGC 7538, G 31.28+0.06, W 75N, S 231, W 51, G 29.95-0.2, and S 269 (Figs. 15 and 16), are consistent with masers occuring at a single radius in an edge-on disk. In the case of S 252, W 48 and Mon R2, the line of sight velocity is not a clear linear function of the major axis position. We are probably observing masers associated with other structures in S 252, e.g the spot at the center of the map could be part of an outflow originating from the disk. In W 48 and Mon R2, the disks could be inclined and masers could arise from a larger range of radii than in e.g NGC 7538. Therefore the v-x diagram is not reduced to a single line. If the masers are in

Table 3. Derived Keplerian parameters: $\frac{M}{r^3}$ deduced from $\frac{dv}{dx}$ in Table 2 and Eq. (2), while diameter of the disk ($d = 2r$) and enclosed mass (M_i) are derived under three cases. Case 1 gives the enclosed mass M_1 assuming that the whole diameter of the disk is given by the observed length in Table 2. The enclosed mass M_2 is calculated in Case 2 by assuming that we only observe a fraction of a disk of 1000 AU in total extent. d_3 in Case 3 is found by taking M=10 $M_\odot$ in $\frac{M}{r^3}$ for each source

Source	Distance	$\frac{M}{r^3}$	Case 1		Case 2		Case 3	
name	(kpc)	($M_\odot$ AU^{-3})	d(AU)	$M_1(M_\odot)$	d(AU)	$M_2(M_\odot)$	d(AU)	$M_3(M_\odot)$
NGC 7538	2.7	9.4×10^{-8}	280	0.25	1000	11.7	940	10
S 252	2.2	3.4×10^{-8}	240	0.06	1000	4.3	1320	10
W 48	3.4	14.5×10^{-8}	1300	6	–	–	–	–
G 31.28+0.06	5.6	0.45×10^{-8}	780	0.26	1000	0.6	2600	10
W 75N	2	3.5×10^{-8}	380	0.24	1000	4.4	1320	10
S 231	2.5	33.4×10^{-8}	95	0.04	1000	41.7	610	10
S 269	4	4.7×10^{-8}	55	0.001	1000	5.8	1200	10
Mon R2	0.83	59.7×10^{-8}	130	0.17	1000	74.6	520	10
W 51	7.5	3.7×10^{-8}	70	0.002	1000	4.6	1300	10
G 29.95-0.02	9	24×10^{-8}	85	0.02	1000	30.8	680	10

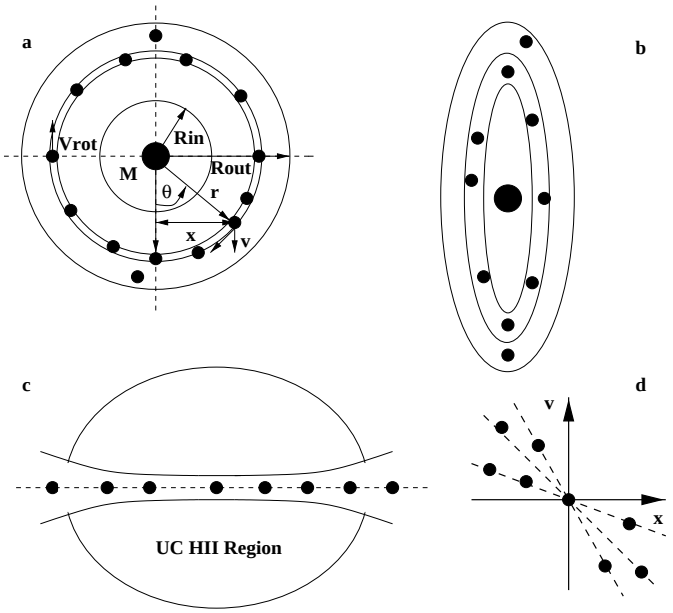

Fig. 17a–d. Maser disk model as proposed by Norris et al. (1998). Small circles indicate masing regions **a** Plan view of maser disk, **b** is a view with a slight inclination of **a** that could explain the elongated morphologies as in W 48. **c** is an edge-on view of **a** that illustrates the linear morphologies as in NGC 7538. Masers might only be observed over a fraction of the disk where the velocity coherence is suitable for masing mechanism. **d** is the velocity vs major axis position diagram for case **c** and **b** in case of a small inclination angle i, where $v = V_{rot} \times \frac{x}{r} \times cosi + v_{sys}$

Keplerian motion within a disk, the velocity gradient measured from the v-x diagram is given by:

$$\frac{dv}{dx} = \sqrt{GM/r^3} \times cosi \quad (2)$$

where M is the enclosed mass. Using Eq. 2, i=0 and the values of $\frac{dv}{dx}$ in Table 2, we derive the measured ratio M/r^3 in the case of a Keplerian disk for all of the disk like structures with the exception of W 48. The values of M/r^3 are given in Table 3 and vary from 4.5×10^{-9} to 5.97×10^{-7} $M_\odot$ AU^{-3}. Our results are consistent with those of Phillips et al. (1998) and Norris et al. (1998) who observed 16 linear structures with velocity gradients out of a total of 45 sources investigated with the ATCA and the Australian VLBI network. However, there is a serious difference in our results when we derive the mass enclosed by the disk (assumed to be the mass of the forming star). Although the velocity gradients which we measure, and hence the values of M/r^3 (10^{-9}-10^{-7} $M_\odot$ AU^{-3}) are similar to those determined by the Australian groups, the linear sizes covered by our Northern sample of masers are up to ten times less. In deriving the enclosed mass, M, our estimate is clearly very sensitive to the assumed radius r. A lower limit to the mass can be derived by assuming that the observed line of masers traces the full diameter of the disk; in this case we find sub-solar masses (see Case 1, Table 3). These limits are much smaller than those obtained by Norris et al. (1998) and Phillips et al. (1998).

4.3. Why do we derive sub-solar masses?

We observe lines of masers from 55 to 780 AU in extent with the exception of W 48 which is 1300 AU. These lengths are ∼7-10 times smaller than those of the lines (585 to 5460 AU) imaged using the ATCA by Phillips et al. (1998). Since we find similar velocity gradients, the derived values of the mass are ∼300-1000 times lower than those in Phillips et al.

Assuming the rotating disk hypothesis to be correct, there are 3 possible explanations for these discrepancies:

1. The methanol masers observed by Phillips et al. each covers a broader velocity range ($\Delta v\sim$ 10-25 km s^{-1}) than those of our Northern sample in which the velocity range is typically $\Delta v\sim$ 5 km s^{-1}. For a given velocity gradient, this broader velocity range corresponds to a greater linear dimension and hence a greater enclosed mass. Since M is proportional to d^3, a factor of 10 in d implies a factor of 10^3 in mass.
2. Resolution differences. The resolution of the EVN and VLBA are considerably finer than that of the ATCA. As a

result the structure observed with the ATCA may be further resolved by the VLBI. For example, in the one source which is common to both our samples, G 9.62+0.20, we observe a different morphology and velocity gradient. While Phillips et al. observe at 6.7 GHz a linear velocity gradient along the whole structure of maser components, our 12.2 GHz data do not exhibit any linear gradient. Although this is a comparison of the 6.7 GHz to 12.2 GHz masers, the similarity of the spectra at both frequencies suggests that the 6.7 and 12.2 GHz maser components should roughly trace the same structure in the VLBI map as seen in NGC 7538, W 48 and S 252.

3. Difference of interpretation of the data, perhaps as a result of the different resolutions. In some cases, Phillips et al. have considered the full extent of the map to represent the diameter of the disk when there is velocity gradient across the map, although the masers do not form a simple elongated structure. We might for example interpret the ATCA maps of G 323.74 and G 337.61 in terms of smaller linear structures and isolated maser clusters rather than single elongated structures.

In conclusion, the selection criteria of the observed maser sources, the higher angular resolution offered by the VLBI and the different ways of interpreting some linear morphologies might explain why we observe smaller lines of masers which are often accompanied with other separated groups of masers instead of large and single morphologies, and hence why we derive sub-solar masses.

4.4. Tracing partial disks around young massive stars

Since most of these methanol masers are closely associated with high mass protostars and UCHII regions, it is reasonable to assume that maser action will occur only in suitable parts of a rotating disk around a young massive stellar object. The masers could trace in some cases only a fraction of the disk in front of the star or at the edges where the velocity coherence along the line of sight is greatest, while in other cases, perhaps as presented in Norris et al. (1998), the masers delineate the full diameter of the disks. For instance if we consider in the case of W 48 that the two axis in Fig. 3 are indeed the minor and major axis of a disk seen with an inclination angle of $\sim 20^o$, then the maser located at the north of the minor axis are all blueshifted with respect to the southern masers. Or the northern masers are receding while the southern masers are approaching. By modelling that structure by a Keplerian disk of diameter $\sim$400 mas or 1300 AU at a distance of 3.4 kpc, and by using the measured velocity gradient (Fig. 15) we find that the enclosed mass is ~ 6 M$_\odot$. In a similar way, we can fit the elongated structure of masers in Mon R2 (see Fig. 9) with a disk inclined at 10^o. Along that disk structure of 160 mas or 130 AU in extent, the velocity is roughly a linear function of the major axis offset position (Fig. 16). Assuming that the whole disk is detected in W 48, we repeat the calculations of Case 1 in Table 3 using the orders of values of M and d observed in W 48. Thus if we assume that the diameter of such disks is about 1000 AU, we can estimate the enclosed mass from the observed ratio $\frac{M}{r^3}$ (see Case 2 in Table 3). Alternately given that massive stars have a mass of $\sim$10 M$_\odot$, we can estimate the diameter of the disk at which the masers occur (see Case 3 in Table 2). We find M between 0.6 and 74.6 M$_\odot$ in Case 2 while the diameter calculated in Case 3 is in the range 520-2600 AU. These results agree with recent observations of rotating disks of a few thousand AU in extent around young massive stellar objects of a few tens of solar masses (see for example, Shepherd & Kurtz 1999, and Cesaroni et al. 1999).

4.5. Tracing outflows or shock fronts

Elongated morphologies and linear velocity gradients are also expected in the case of masers tracing bipolar outflows, e.g bipolar maser emission from HD101584 (Te Lintel Hekkert et al. 1992). Although there is no theoretical support for Class II methanol masers forming in such environment, the observed linear morphologies could trace collimated outflows originating from a protostar. It has been mentioned in Sect. 3.5 as a possible explanation of the linear structure in W 75N that aligns on the line of H_2O and OH masers. Linear morphologies could be parts of outflows, not necessarily the inner part originating from the stars, but only where the conditions are the most suitable to form methanol masers.

Another possibility to explain the line of masers is to consider that they form in the layer between the ionisation and shock fronts surrounding the UCHII region. In that case no linear velocity gradient is required along the line of masers that forms tangentially to the shock front. Such a hypothesis may explain the case of G 9.62+0.20 where there are two lines of masers without any linear velocity gradient (see Fig. 10). These 2 lines of masers may arise from the expanding front surrounding the UC HII region as OH masers are sometimes found to do (Forster & Caswell 1989).

5. Conclusions

We have mapped the spatial distribution of the 6.7 and 12.2 GHz methanol masers in 14 star-forming regions. The VLBI maps of 10 out of these 14 sources reveal elongated structures of masers with linear velocity gradients along them, compatible with rotating disks seen almost edge-on. This confirms recent observations of methanol masers by Norris et al. (1998) and Phillips et al. (1998). If we are seeing the whole diameter of the methanol maser disk then we derive sub-solar enclosed masses. A more likely explanation of our results is that we only see a fraction of the rotating disk around young massive stars, and therefore derive central masses which are too small. For instance, assuming that the disks have a diameter of $\sim$1000 AU as found in W 48, we estimate the central mass M between 0.6 and 74.6 M$_\odot$. We stress that the disk model is not the only possible scenario. Masers forming in outflows and behind shock fronts could also explain some of the observed geometrical structures. Proper motion studies have been undertaken in order to validate

the most suitable model in five sources and will be presented in forthcoming papers.

Acknowledgements. We thank the observatories of the US and European VLBI Networks for their assistance during these observations. We also thank Chris Phillips for communicating us the absolute position of a few objects.

References

Baart E.E., Cohen R.J., Davies R.D., Norris R.P., Rowland P.R., 1986, MNRAS 219, 145
Blum R.D., Damineli A., Conti P.S., 1999, ApJ 117, 1392 Braz M.A., Sivagnanam P., 1987, ApJ 181, 19
Braz M.A., Sivagnanam P., 1987, A&A 181, 19
Carpenter J.M., Meyer M.R., Dougados C., Strom S., Hillenbrand L., 1997, ApJ 114, 198
Carpenter J.M., Sanders D.B., 1998, ApJ 116, 1856
Caswell J.L., Gardner F.F., Norris R.P., et al., 1993, MNRAS 260, 425
Caswell J.L., Vaile R.A., Ellingsen S.P., Whiteoak J.B., Norris R.P., 1995, MNRAS 272, 96
Cesaroni R., Hofner P., Walmsley C.M., Churchwell E., 1998, A&A 331, 709
Cesaroni R., Felli M, Jenness T., et al., 1999, A&A 345, 949
Eiroa C., Casali M.M., Miranda L.F., Ortiz E., 1994, ApJ 290, 599
Forster J.R., Caswell J.L., 1989, A&A 213, 339
Genzel R., Downes D., 1977, A&AS 30, 145
Haikala L.K., 1995, A&A 294, 89
Haschick A.D., Reid M.J., Burke M.J., Moran J.M., Miller G., 1981, ApJ 244, 76
Hofner P., Kurtz S., Churchwell E., Walmsley C.M., Cesaroni R., 1996, ApJ 460, 359
Hughes V.A., 1985, ApJ 298, 830
Hunter T.R., Taylor G.B., Felli M., Tofani G., 1994, A&A 284, 215
Israel F.P., Felli M., 1978, A&A 63, 325
Kurtz S., Churchwell E., Wood D.O.S, 1994, ApJS 91, 659
Lada C.J., Blitz L., Reid M.J., Moran J.M., 1981, ApJ 243, 769
Lin D.N.C., Pringle J.E., 1990, ApJ 358, 515
Menten K.M., 1991, ApJ 380, L75
Migenes V., Cohen R.J., Brebner G.C., 1992, MNRAS 254, 501
Minier V., Booth R.S., Conway J.E., 1998, A&A 336, L5
Minier V., Booth R.S., Conway J.E., 1999, NewAR 43, 569
Miralles M.P., Salas L., Cruz-González I., Kurtz S., 1997, ApJ 488, 749
Moscadelli L., Menten K.M., Walmsley C.M., Reid M.J., 1999, ApJ 519, 244
Norris R.P., McCutcheon W.H., Caswell J.L., et al., 1988, Nat 335, 149
Norris R.P., Whiteoak J.B., Caswell J.L., et al., 1993, ApJ 412, 222
Norris R.P., Byleveld S.E., Diamond P.J., et al., 1998, ApJ 508, 275
Onello J.S., Phillips J.A., Benaglia P., et al., 1994, ApJ 426, 249
Phillips C.J., Norris R.P., Ellingsen S.P., McCulloch P.M., 1998, MNRAS 300, 1131
Reid M.J, 1995, In: Zensus J.A., Diamond P.J., Napier P.J. (eds.) ASP Conference Series 82, Very Long Baseline Interferometry and the VLBA. PASP, San Francisco, p. 209
Shepherd D.S., Kurtz S.E., 1999, ApJ 523, 690
Slysh V.I., Val'tts I.E., Kalenskii S.V., et al., 1999, A&AS 134, 115
Snell R.L., Bally J., 1986, ApJ 303, 683
Snell R.L., Huang Y.-L., Dickman R.L., Claussen M.J., 1988, ApJ 325, 853
Sobolev A.M., Cragg D.M., Godfrey P.D., 1997, A&A 324, 211
Te Lintel Hekkert P., Chapman J.M., Zijlstra A.A., 1992, ApJ 390, L23
Testi L., Felli M., Persi P., Roth M., 1998, A&A 329, 233
Torelles J.M., Gómez J.F., Rodriguez L.F., et al., 1996, ApJ 457, L107
Torelles J.M., Gómez J.F., Rodriguez L.F., Curiel S., Vásquez Roberto, 1997, ApJ 489, 744
Vallée J.P., Avery L.W., 1990, A&A 233, 553
Walsh A.J., Hyland A.R., Robinson G., Burton M.G., 1997, MNRAS 291, 261
Walsh A.J., Burton M.G., Hyland A.R., Robinson G., 1998, MNRAS 301, 640
Watson A.M., Hanson M.M., 1997, ApJ 490, L165
Wood D.O.S., Churchwell E., 1989, ApJ 340, 265
Zhang Q., Ho P.T.P., Ohashi N., 1998, ApJ 494, 636